Mode-locked rotating detonation waves: Experiments and a model equation

James Koch, Mitsuru Kurosaka, Carl Knowlen, and J. Nathan Kutz

Phys. Rev. E **101**, 013106 — Published 10 January 2020

DOI: 10.1103/PhysRevE.101.013106

Mode-Locked Rotating Detonation Waves: Experiments and a Model Equation

James Koch,* Mitsuru Kurosaka, and Carl Knowlen
William E. Boeing Department of Aeronautics and Astronautics, University of Washington, Seattle, WA 98195-2400

J. Nathan Kutz
Department of Applied Mathematics, University of Washington, Seattle, WA 98195-3925

Direct observation of a Rotating Detonation Engine combustion chamber has enabled the extraction of the kinematics of its detonation waves. These records exhibit a rich set of instabilities and bifurcations arising from the interaction of coherent wave fronts and global gain dynamics. We develop a model of the observed dynamics by recasting the Majda detonation analog as an autowave process. The solution fronts become attractors of the engine; i.e., mode-locked rotating detonation waves. We find that denotative energy release competes with dissipation and gain recovery to produce the observed dynamics and a bifurcation structure common to other driven-dissipative systems, such as mode-locked lasers.

I. INTRODUCTION

The *Rotating Detonation Engine* (RDE) is a thrust-producing device in which self-sustained combustion-driven shock waves, or detonations, travel azimuthally in an annular combustion chamber. Pressure rises through the detonation process, contrasting conventional deflagration-based engines. Successful implementation of so-called 'pressure gain' combustion implies mechanical simplification of propulsion systems (for example, pumping requirements for propellant can be reduced [1]) and an increase of available work for a given propellant over conventional engines [2], ultimately resulting in fuel savings. However, a diverse set of experimentally observed instabilities and bifurcations are known to be ubiquitous in RDEs [3–5], potentially compromising performance and stable operation. In this article, we develop a modeling framework that characterizes the underlying global bifurcation structure of RDEs, showing that the nonlinear dynamics are governed by the interaction physics of global gain (fuel) depletion and recovery along with local dominant balance physics characterized by the Burgers' equation [6]. Our predictions capture the cascade of bifurcations and flame-front solutions whose attracting nature we term *mode-locked rotating detonation waves* and which are observed experimentally within the RDE. Further, the model shows that the underlying energy balance physics of the driven-dissipative RDE mimics those of mode-locked lasers [7, 8], where global gain dynamics produce a similar cascading bifurcation diagram of mode-locked states [9].

Conventional RDEs use concentric cylinders to direct the flow of propellant into a narrow annular gap (see Fig. 1). Inside this gap, an igniter deposits concentrated energy into the propellant mixture, creating an ignition kernel that promotes the exothermal chemical reaction.

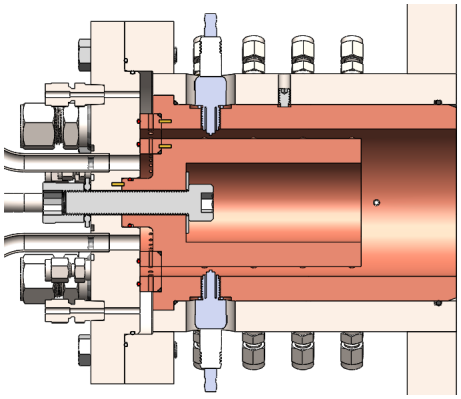

FIG. 1. (Color online) Section view of the Rotating Detonation Engine (RDE) used for this study. The engine geometry is such that gaseous methane and oxygen is directed into a narrow annular gap through a set of propellant injectors. A spark plug ignites the mixture, which rapidly transitions to a number of circumferentially traveling detonation waves.

By virtue of the narrow annular gap, the gradients in density and pressure caused by the heat release self-steepen, eventually forming shocks strong enough to auto-ignite the propellant. These combustion-driven shock waves, now detonations traveling at speeds on the order of km/s, continue to process propellant so long as there is sufficiently fast refill and mixing of propellant within the period of the traveling detonation wave to offset inhibiting phenomena [10, 11]. In this manner, the steady operation of the RDE is the point at which the rates of gain depletion (combustion), gain recovery (injection and mixing), and dissipation (exhaust and energy ejection) balance. For these to exist in an unbalanced state induces a degree of unsteadiness, typically manifested as a transition to a different number of waves or modulation of wave speed [3–5, 12]; i.e., the system bifurcates.

In laboratory experiments, typical observables are wave count, speed, and direction as captured by pressure

* jvkoch@uw.edu

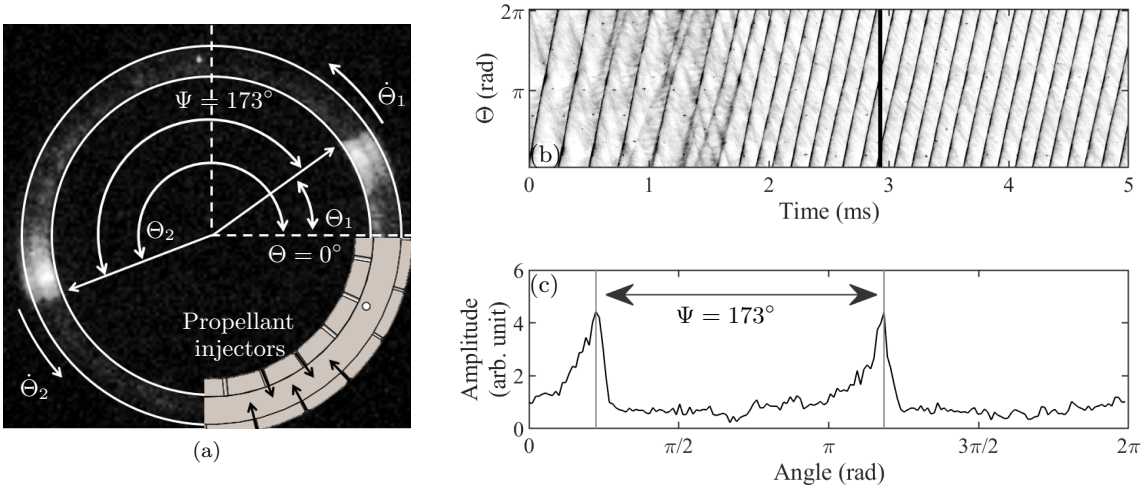

FIG. 2. (a) A high-speed camera frame from an experiment shows the location of rotating detonation waves in the annulus of a RDE. Overlaid is a rendering of the propellant injection scheme. (b) Tracking the detonations through time yields a spatial-temporal view of their kinematics. Line slopes correspond to speed. The vertical cut in (b) is synchronized with the states of (a) and (c). (c) The phase difference Ψ for the waves seen in (a) is not π, though eventually the phase difference approaches this stable value.

sensors or optical instruments. Common in experimental literature are a few themes: (i) the observed detonation wave speeds are significantly less than the Chapman-Jouget (CJ) velocity (the steady, shock-induced combustion wave in which the combustion products are sonic relative to the wave front) for the propellant mixture [13, 14], (ii) the number of waves is tied to the mass flux of propellant through the engine and the propellant injection scheme [11, 15], and (iii) parasitic combustion, meaning deflagration not associated with a traveling wave, is ubiquitous [5, 12, 14]. We note that to fully realize theoretical performance gains in RDEs, such non-detonative heat release must be minimized. Additionally, we acknowledge the prevalence of counter-propagating waves in literature (see [5] and [14]). However, for the present article we restrict our discussion to co-rotating waves only as a means to simplify the modeling and analysis.

Computational fluid dynamic modeling of RDEs allows for detailed investigations of the wave structure and engine flowfield. Not only do these models agree well with experiments, but they also produce many of the instabilities and observed bifurcations of RDEs, including mode-locked states [16–19]. However, these high-fidelity simulations are computationally expensive; i.e., to extract limit cycle behavior of the wave dynamics and bifurcation structures is not currently feasible. Additionally, they fail to identify the leading order physics responsible for producing the bifurcations. Our modeling efforts draw on recent experimental observations of nonlinear dynamics of rotating detonation waves to formulate a reduced-order model that captures the bifurcations observed in practice. We have identified the dominant energy balance physics responsible for producing the universally observed physics of the mode-locked states and their interactions in many RDEs. Indeed, the primary bifurcation parameter controlling the cascade of bifurcations is easily identified as the propellant injection and mixing rate. The energy balance physics is canonical in that it is prevalent in a broader range of driven-dissipative physical systems, including mode-locked lasers [7–9, 20], Bose-Einstein condensates (BECs) [21], and some biological systems [22]. Such rich bifurcation structures pervade spatio-temporal systems driven to instability [23].

In Section II, we describe the experimental apparatus and display recent observations of nonlinear dynamics within the engine. Building on these observations, a model system is proposed in Section III with a goal of reproducing, qualitatively, the observed dynamics. Numerical experiments of the proposed model are presented in Section IV and follow with a discussion of the model and observations in Section VI.

II. EXPERIMENTS

For the present study, an RDE (Fig. 1) and test cell were designed and constructed to investigate rotating detonation wave dynamics. The engine used for this study is unique in that the engine internal components are modular. Engine cores can be swapped out to give different annular gaps and combustor lengths. The injectors can be similarly exchanged to investigate injector-combustion coupling and mixing strategies. The test cell is a backpressure controlled facility. Engine exhaust is routed to an appropriately sized vacuum chamber with a known backpressure. The test cell is optically accessible, which allows for recording the complete kinematic history of all detonation waves with high spatiotemporal resolution (Fig. 2a). Each experiment is a 0.5 second burn of a

known proportion and feed rate of gaseous methane and oxygen. In a successful experiment, a spark ignites the mixture and produces an accelerating flame that transitions into a number of traveling detonation waves. A complete description of the experimental apparatus and procedures are detailed in [24].

A fundamental assumption of this study is that the observed luminosity in these experiments correlates to combustion progress, meaning brighter regions exhibit higher heat release than darker regions. Supposing this to be true, we examine example waveforms extracted from the high-speed camera footage. For each experiment, the azimuth-time history is extracted from high-speed video footage through a pixel-intensity integration algorithm [25]. The wave kinematics can be recorded in this manner and displayed as a $\theta - t$ diagram, an example of which is shown in Fig. 2b. Furthermore, these records can be recast in the wave-attached frame, in which case the phase differences between waves is an explicit output (the tracked wave appears steady in this reference frame). Figure 3a is the data in Fig. 2b shifted to the wave reference frame. The corresponding velocity of the tracked wave is displayed in Fig. 3c. For these figures, we nondimensionalize time as $\tau = t\,(D_{wave}/L)$, where L is the length of the periodic domain and D_{wave} is the speed of the wave in its mode-locked state.

In Fig. 3a, an observed transition from one wave to two waves during the startup transient is shown. In this mode transition, after a point of criticality, a second detonation wave forms and begins to travel around the annulus. However, the spacing between the two waves in the annulus is asymmetric, causing an imbalance in the amount of propellant consumed by each of the waves. The wave with coordinate θ_1 trailing the preceding wave θ_2 exists with a phase difference of $\Psi = \theta_2 - \theta_1 < \pi$ (see Fig. 2a). At that instant, assuming the propellant refresh rate is approximately constant, the trailing wave has less than half of available propellant in the chamber for its consumption. The local balance of gain (heat release), gain recovery (injection and mixing), and dissipation (energy ejection processes) is not satisfied. Since propellant heat release directly affects the speed of a detonation, the trailing wave begins to decelerate. The preceding wave, however, can process the remaining portion of available propellant and accelerates through this excess. In this manner, these two waves behave dispersively, where they seek a stable state with maximum and symmetric phase differences. For the single wave portion in Fig. 3a, the quasi-steady wave has a velocity 20% to 30% below the Chapman-Jouget velocity for the propellant mixture. This metric is a direct observable of the energy necessary to sustain the detonation wave subject to dissipation and gain recovery in the combustion chamber. As the transition to two waves occurs and the dynamics settle to a steady state, the wave speed reduces to about 90% of the single wave speed.

The opposite scenario occurs upon ramp-down of propellant feed at the end of each experiment. Figure 4a

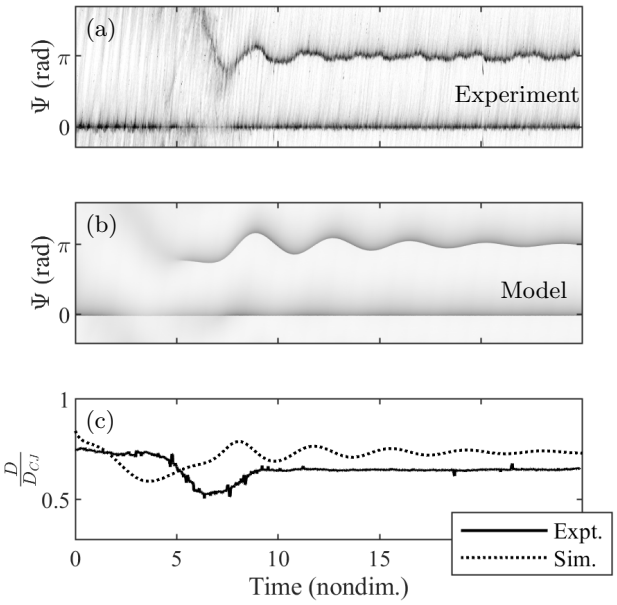

FIG. 3. Representative wave nucleation process in a startup transient in an experiment (a) and in a simulation of the proposed model (b) displayed as pseudocolor plots of amplitude (arb. units). As seen in the wave reference frame of (a) and (b), the oscillatory phase difference between the two waves immediately after nucleation decays through time as the two waves become mode-locked. (b) corresponds to $s = 3.5$. The instantaneous speeds of the waves along $\Psi = 0$ in (a) and (b) are given in (c).

exemplifies a ramp-down transition of 2 to 1 wave over the span of about 10 ms. The two waves compete for the increasingly scarce propellant, as opposed to the case of excessive propellant exhibited in Fig. 3a. Because of an initial perturbation in phase difference, the waves begin to exchange strength (speed and amplitude) in a regular fashion producing the exponential instability growth. As the phase difference oscillations grow, a catastrophic interaction between the waves occurs, resulting in the overrunning of the weaker wave by the stronger wave during one of the large-amplitude oscillations. After the bifurcation, the velocity of the remaining wave is about 10% higher than that of the wave prior to the instability.

Wave instabilities that do not lead to a change in the number of waves are common in the tested set of hardware. Fig. 5 exhibits a periodic wave velocity and amplitude observed in an experiment with three co-rotating waves. This is a clear modulational instability as spectral sidebands accompany the carrier frequency corresponding the the mean traveling wave velocity in the combustion chamber. This mode of operation is stable in the sense that it does not lead to a bifurcation of number of waves unless the flow condition is perturbed significantly.

Pulsating modes of operation have also been observed in some experiments with very large injector areas (rel-

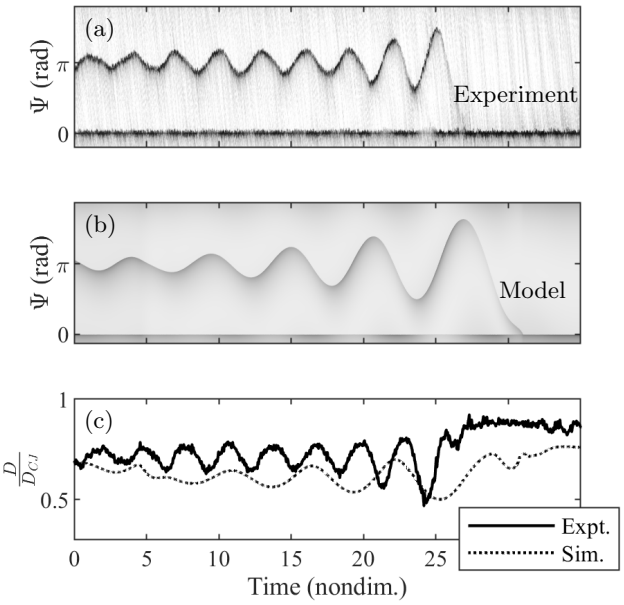

FIG. 4. Representative destruction of a wave in an experiment (a) and in a simulation of the model (b) shown in the wave-attached reference frame as pseudocolor plots of amplitude (arb. units). Oscillations in Ψ grow exponentially until one wave overruns the other. For a given injection function β and loss ϵ, the oscillation period and phase difference growth rate are parameterized by the change in s and u_p. (b) corresponds to $s = 2$ with a -20% change in s applied to the mode-locked state. The instantaneous speeds of the waves along $\Psi = 0$ in (a) and (b) are given in (c).

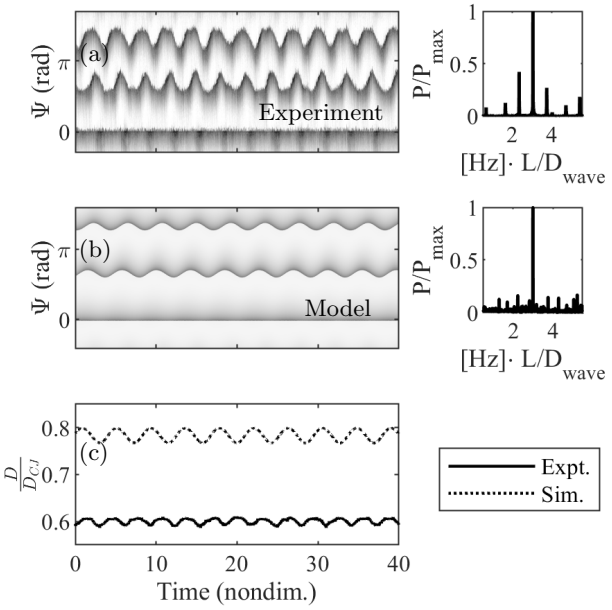

FIG. 5. Space-time history of mode-locked modulation of wave speeds an experiment (a) and in a simulation (b) in the wave reference frame. The instantaneous speeds of the waves along $\Psi = 0$ in (a) and (b) are shown in (c). The accompanying spectra show clear sidebands symmetric about the carrier frequency. The frequency shown in the spectra is scaled by the average transit time of the mode-locked wave, L/D_{wave}. The abscissa magnitude corresponds to a count of the waves in the domain. As shown, the dominant frequency is three waves with sidebands near two and four waves.

ative to the area of the annular combustion chamber). This mode of operation is characterized by a binary 'on/off' behavior of the injectors and subsequently mixing and combustion. The oscillatory plane waves from an example pulsating mode is given in Fig. 6.

III. A QUALITATIVE MODEL

We propose a model that captures the dominant physics involved in the processes of wave formation, mode-locking, and mode bifurcations for further study of these phenomena. The detonation analogs of Majda [6], Fickett [26], Rosales [27], and Faria and Kasimov [28] have enabled the rigorous mathematical description of detonation stability [29] and detonation dynamics in one (limit cycles and chaos) and two dimensions (cells and pattern formation). These analyses typically occur in the Lagrangian, shock-attached framework under assumptions of complete combustion. We use the formulation of Majda's analog as a starting point as it sufficiently captures the dominant shock-chemistry interplay found in detonation waves. Specifically, we aim to recast Majda's analog in terms of autowave-producing variables [30, 31]. Our model captures the dominant physics of gain depletion, gain recovery, and dissipation whose structure is given by:

$$\frac{\partial \eta}{\partial t} + \eta \frac{\partial \eta}{\partial x} = (1-\lambda)\,\omega(\eta)\,q_0 + \epsilon\xi(\eta) \tag{1a}$$

$$\frac{\partial \lambda}{\partial t} = (1-\lambda)\,\omega(\eta) - \beta(\eta, \eta_p, s)\,\lambda. \tag{1b}$$

In keeping with the convention of the field of detonation analogs, $\eta(x,t)$ is an intensive property of the working fluid (here taken to be specific internal energy - see [6] and [32]) and λ is a combustion progress variable ($\lambda = 0$ is unburnt and $\lambda = 1$ is complete combustion). Gain is modeled with a heat release function, $\omega(\eta)$ with heat release q_0 as a proportionality constant. Losses are modeled with a generic loss function $\epsilon\xi(\eta)$ where ϵ is a loss magnitude constant. Lastly, the gain recovery is dictated by the injection model $\beta(\eta, \eta_p, s)$, where η_p and s are injection parameters. The domain is restricted to a 1-D periodic line in the Eulerian reference frame. A control volume-based derivation of the model system is provided in Appendix A.

The exact functional forms of the gain depletion, gain recovery, and loss terms are not critical to produce mode-locked rotating detonation waves. However, the inclusion of each of these terms in the model system is critical - to

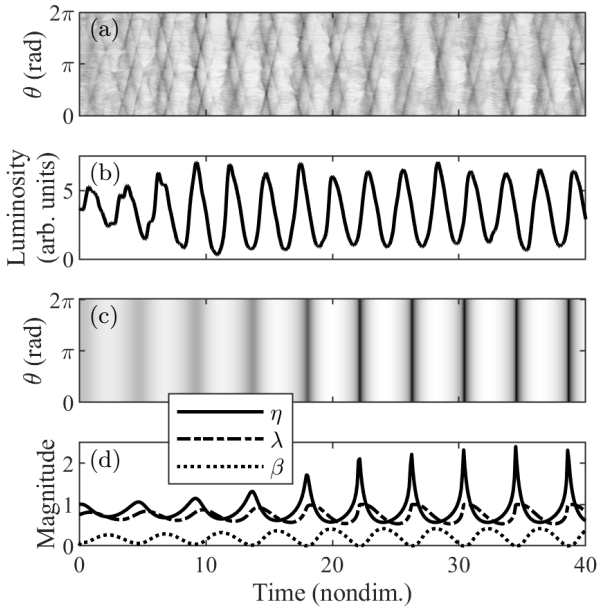

FIG. 6. Space-time history of plane wave pulsation mode of operation in an experiment (a,b) and in a simulation (c,d). Simulation parameters are those listed in Table I with $q_0 = 6$ and $\epsilon = 1.0$. The deactivation and reactivation of the injectors gives rise to a resonance between the combustion and propellant injection.

omit any one will destroy the balance required to provide the necessary properties and dynamics relevant to RDEs. In the opinion of the authors, presented herein are the simplest viable functional forms to provide the dynamics observed in real engines. These terms undoubtedly require modifications and/or parameter changes to mimic a specific set of hardware, but the underlying physical principles modeled by these terms are hypothesized to persist among all RDEs.

Gain Depletion

The heat release function $\omega(\eta)$ is dictated by a simplified version of Arrhenius kinetics with a explicitly defined 'ignition energy' η_c, activation energy α, and pre-exponential factor k:

$$\omega(\eta) = k e^{\left(\frac{\eta-\eta_c}{\alpha}\right)}. \tag{2}$$

For a steadily traveling detonation wave, the expectation is that this gain term dominates the dynamics, providing a rapid release of energy into the domain saturable only by exhaustion of fuel or another nonlinear effect (such as a nonlinear loss term).

Losses

The loss of energy in the domain is taken to be a generic restoring force to a natural state by thermal conduction or energy advection processes. Assuming the working fluid has constant specific heat at constant volume (c_v), one can relate states of internal energy (η) to temperature (T) by $\eta_2 - \eta_1 = c_v (T_2 - T_1)$. Therefore, we model heat conduction by:

$$\epsilon\xi(\eta, \eta_0) = \epsilon(\eta_0 - \eta), \tag{3}$$

where the proportionality constant ϵ assumes responsibility for the specific heat of the fluid and heat transfer coefficient and η_0 is the ambient state of the system.

Advection of energy away from the domain is modeled by an imposed axial pressure gradient that ejects flow from the combustor (see Appendix B) whose form is given by:

$$\epsilon\xi(\eta) = -\epsilon\eta^2. \tag{4}$$

These loss functions are generic in that the relative significance of losses compared to gain can be modified by the proportionality constant ϵ. In this paper, we explore both linear (heat conduction) and quadratic (energy advection) losses independently. For simplicity, we take $\eta_0 = 0$ such that the loss terms become $-\epsilon\eta$ or $-\epsilon\eta^2$ in the linear and quadratic loss cases, respectively.

Gain Recovery

The gain recovery term $\beta(\eta, \eta_p, s)$ works against gain depletion to 'refill' the domain towards a $\lambda = 0$ state. In gaseous injection, injectors are typically 'choked' orifices, meaning that perturbations in the combustor cannot influence the injection process as no characteristics can travel upstream past the choke point. However, in the presence of large-amplitude pressure oscillations (such as those present in detonation engines), the peak pressures may be comparable to those of the propellant plenums. This implies a loss of the sonic condition of the injectors. Should this occur, the state of the combustor becomes coupled to the injection scheme and can lead to unsteady behavior. In RDEs, the pressures generated by the detonation waves can be an order of magnitude larger than the propellant feed pressures. The injectors are periodically blocked (cutoff of injection) and backflow may be induced into the plenum chambers, further disrupting the injection process. To include these phenomena into the model, we use an activation function-based injector term that responds to the periodic forcing by the rotating detonation waves. The proposed activation function is given by:

$$\beta(\eta, s) = \frac{s}{1 + e^{r(\eta-\eta_p)}}, \tag{5}$$

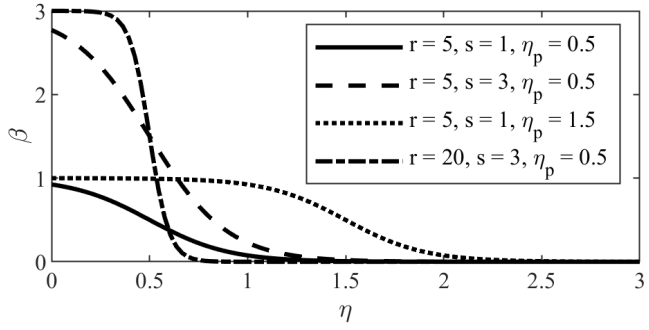

FIG. 7. The influence of the state of the domain, η, on the gain recovery function β following the functional form of Eq. (5). The solid line is the activation function used for simulations in Section IV.

TABLE I. Simulation Parameters

L	q_0	α	η_c	η_0	η_p	k	ϵ	r	D_{CJ}
2π	1.0	0.3	1.1	0	0.5	1	0.11	5	2

where s is a parameter analogous to injection area, η_p is the injector 'plenum pressure', and r is a parameter adjusting the 'steepness' of the activation function. Increasing injection area (s), plenum pressure (η_p), or both increases the mass flux into the engine. However, the dynamic response to these increases differs significantly. In the case of a high plenum pressure (a 'stiff' injector), the influence of the detonation pressure becomes insignificant and the injector can deliver a consistent supply of propellant. In the case of a large injection area (holding the plenum pressure constant), the injectors are susceptible to large fluctuations of mass flux in response to this periodic forcing. Example activation function-based injector models are shown in Fig. 7. Mixing is assumed to be exponential with time - in the absence of combustion, λ asymptotically approaches 0.

IV. NUMERICAL EXPERIMENTS

Numerical simulations are performed with the PyClaw open source finite volume software [33] on a converged grid. The parameters used for the numerical simulations in this article are given in Table I. Exceptions are noted as appropriate.

Planar Fronts

We first examine the existence of planar solutions to the model system, including limit cycle behavior. The initial value problem was solved with initial condition $\eta(x,0) = 1$ and $\lambda(x,0) = 0.75$. A plane wave oscillates about the point in phase space where gain depletion and gain recovery match ($\beta\lambda = (1-\lambda)\omega(\eta)$) subject to the balance of energy input and energy rejection and dissipation ($\epsilon\xi = (1-\lambda)\omega(\eta)q_0$). Low-energy oscillations decay to a planar deflagration front without oscillations. Pulsating fronts, such as those seen in recent experiments, are characterized by periodic 'activation' and 'deactivation' of the injectors - first resonating with the heat release, and subsequently saturated by the loss mechanisms. An example of a plane wave pulsating front can be seen in Figure 6d for a single location in the annulus through time. The corresponding space-time history for the pulsating mode of operation is given in Figure 6c. Pulsating plane wave solutions of the full model are stable for planar initial conditions, but are unstable to perturbations as they grow into traveling detonation waves.

Traveling Waves

For traveling wave simulations, the initial value problem with initial condition $\eta(x,0) = (3/2)\text{sech}^2(x - x_o)$ and $\lambda(x,0) = 0$ was solved under varying refill (s, holding η_p constant) conditions and with linear and nonlinear loss terms.

As in [6], we find the analogous CJ velocity of the reduced system (the inviscid, steady wave in which all energy has been released to the wave in a infinitesimally thin reaction zone). This steady wave speed is defined as the minimum speed that fulfills the Rankine-Hugoniot conditions for the prescribed heat release. In the absence of losses, this minimum speed (CJ velocity, D_{CJ}) is $D_{CJ} = (\eta_1 + q_0) + \sqrt{q_0\,(q_0 + 2\eta_1)}$, where η_1 is the upstream state of a steady, shock-attached framework of the Majda Model. In the case of $\eta_1 = 0$, the speed of the CJ wave becomes $D_{CJ} = 2q_0$. This speed is the metric upon which the traveling waves in the proposed model are benchmarked.

The evolution of a typical simulation is given in Fig. 8. Because the initial *sech*-pulse is well above η_c, the medium locally and rapidly releases heat. The wave steepens and forms a detonation. This initial pulse travels at the CJ speed until it reaches its tail, at which point the wave begins to rapidly dissipate and decelerate: the limited amount of gain recovery cannot continue to sustain the wave at $D_{CJ} = 2q_0$. Additionally, the rapid heat release (compared to the time scale of the dissipation of energy) of the initial CJ wave acts to raise the average η in the domain substantially above the ambient value η_0 and ignition value η_c. In this manner, the *effective* activation energy of the active medium is lowered and parasitic deflagration, or slow-scale heat release not associated with the traveling waves, is promoted in the entirety of the domain. Because the transit time of the initial traveling wave has been increased through dissipation, the parasitic deflagration has ample time to complete the deflagration-to-detonation (DDT) process and form multiple, lower amplitude detonation waves.

To induce a mode transition from an already mode-locked state, a step change in s is applied to the steady state, inducing a bifurcation. An example of such a tran-

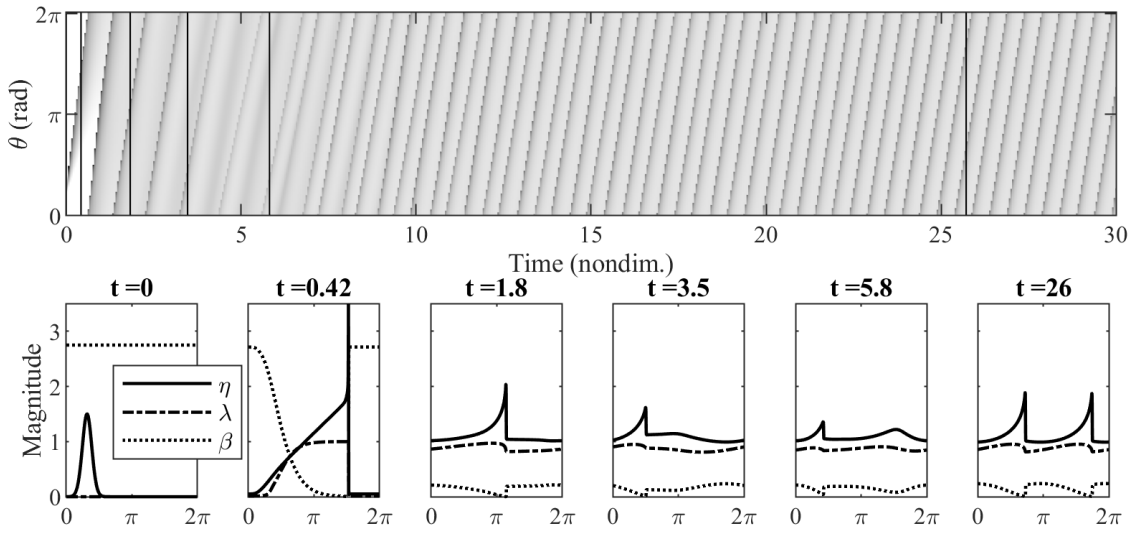

FIG. 8. Nucleation and mode locking of detonations from a single pulse initial condition ($s = 3.5$). Vertical lines in the $\theta - t$ diagram correspond to simulation snapshots shown. The initial *sech*-pulse rapidly transitions to a CJ detonation. In regions where η is low, the injectors behave steadily. However, as the wave reaches its tail, η is everywhere elevated and the injection is severely curtailed. A second wave forms from the self-steepening of parasitic deflagration. After wave nucleation, the two waves behave dispersively and their phase differences approach π.

sition is shown in Fig. 4b, where two initially mode-locked rotating detonation waves become unstable and destructively bifurcate. Low-amplitude phase difference oscillations grow exponentially, much like the experimental observations in Fig. 4a. During the period of oscillations, the two waves exchange strength (amplitude) and speed. For a given injection function β and loss ϵ, the instability growth rate and oscillation period is parameterized by the severity of the applied step in s and η_p.

Upon nucleation of a new wave or destruction of an existing wave, the collection of waves in the chamber act dispersively, eventually forming a mode-locked state. The spatial imbalance of gain and dissipation in the domain allows for the characteristic modulation of detonation wave speed and amplitude. In transients of gain recovery, such as when the mass flow rate of an experiment is not constant, seen is a local imbalance of the gain and dissipation that either nucleates a new wave or amplifies asymmetric perturbations between waves, eventually causing a catastrophic destructive interaction.

Bifurcation diagrams showing the dependence of number of waves, wave speed, and wave amplitude on s and the loss term is shown in Fig. 9 for the parameters of Table I. As s is increased from zero, steady planar deflagration fronts form for small values. Once the value of s can support a traveling wave, the waves follow the staircase behavior in Fig. 9, where the wave speed increases until another bifurcation occurs. These waves nucleate from the parasitic deflagration through a DDT process (as in Fig. 3b and 8). At each bifurcation to an increased number of waves, there is a drop in wave speed, though this drop in speed becomes less severe as the number of waves increases. This phenomena is consistent with the presented experiments as well as the observations of many in the literature [11]. In the limit as s becomes large, the number of waves increases until the wave fronts are low in amplitude (relative to the mean state of the domain) and merge into a planar deflagration front.

For sweeps of the bifurcation parameter s with an imposed quadratic loss, a series of period-halving bifurcations increase order in the system (from chaotic propagation to constant wave phase differences) during the transition from one to two waves (Fig. 9d). In the regime of chaotic propagation, there is aperiodic nucleation, destruction, and modulation of the waves. As the gain is increased, the waves transition to periodic modulation of wave speed and phase difference. This characterisitic modulation is also seen in the transition from two to three waves (as in Fig. 5). These intermediate modes are stable (persist for long durations). A significant degree of hysteresis is also noted in the regions near mode changes. Approaching criticality for any bifurcation-inducing parameter from above or below gives different behavior near the bifurcation. For example, a portion of the chaotic region in Fig. 9 exhibits single-wave and dual wave chaotic multistability depending on a single or double wave initial condition.

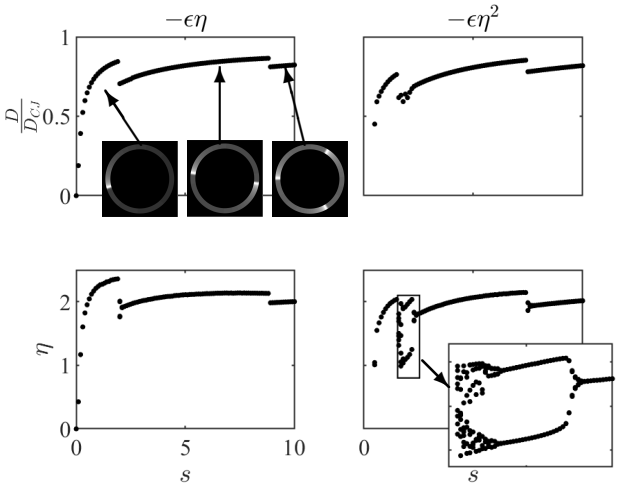

FIG. 9. Number of waves and wave speed through a sweep of the bifurcation parameter s for linear and nonlinear loss terms. The final states have been approached from 'above'; i.e., via a relaxation of three waves to two or one waves. In the transition from one to two waves for the nonlinear loss case, a series of period-halving bifurcations increase order in the system to eventually form two mode-locked waves with zero oscillation in phase difference. The qualitatively similar experimental bifurcation structure is published in Bykovskii et al. [11]. The energy balance dynamics in laser cavities produce a similar cascaded bifurcation structure, including chaotic inter-pulse regimes [9, 34].

V. DISCUSSION

The model system presented in this paper qualitatively reproduces the nonlinear dynamics of collections of rotating detonation waves observed in experiments. The proposed system is an adaptation of the Majda detonation analog to a periodic domain with gain depletion, gain recovery, and generic restoring forces included in the system. These terms sufficiently mimic real-engine processes such as heat release, propellant injection, and rejection of energy to an ambient condition. While we have not explicitly captured all physical processes involved in real engines, nor have we perfectly identified the functional forms for the included terms, we do claim to have identified the dominant balance physics involved in the nonlinear dynamical behavior seen in real engines. These phenomena include wave nucleation (Fig. 3), mode locking of multiple waves (Fig. 8), wave destruction (Fig. 4), wave modulation (Fig. 5), and pulsating plane waves (Fig. 6).

In this section, we wish to emphasize several of the key findings of this study. First is the establishment of the communication pathways and dispersive properties of the collection of waves within the domain. Second, we establish the acceleration of chemical kinetics, subject to weak loss terms, as the physical mechanism responsible for parasitic deflagration and wave front bifurcations. Lastly, we relate the rotating detonation wave phenomenon to the more established field of mode-locking in driven-dissipative systems.

A. Communication Pathways

In steady operation of an RDE and in the mode-locked state of the proposed model system, a number of traveling detonation waves co-exist in the periodic domain with maximum possible phase differences between the waves. Supposing these traveling waves to be detonations, there is an implied lack of communication between the waves: detonations travel supersonically and, if steady, in a condition where the combustion products are sonic relative to the wave front. For the waves to behave dispersively, as in Figs. 3 and 4 near the bifurcation points, implies a significant communication pathway or coupling mechanism in an apparent contradiction to standard detonation theory. We note that the propellant injection scheme is responsible for providing a consistent combustible medium through which the detonations can propagate. However, known is that detonations induce blockages or backflow into propellant plenums. This phenomena is captured in our proposed functional form of β in Eq. (5), providing a necessary feedback mechanism between the detonations and the injection scheme. In this manner, the presence of all detonation waves is impressed upon the dynamic response of the injection scheme and long-range communication is established, allowing for dispersive behavior of the detonation waves. We therefore conclude that the coupling of the injectors and the detonation waves is the physical mechanism that drives the observed dynamics in both experiments and in the proposed model, subject to the constraint of the generic losses inside of the chamber. In the presence of this non-locality, domain periodicity, and nonlinear energy balance, chaotic solutions have been found to exist, as shown in Fig. 9.

B. Bifurcations and Arrhenius Kinetics

The presence of parasitic deflagration and weak restoring forces are the key physical mechanisms identified in the model system for inducing bifurcations. Within the model system, the time scale for detonative energy release is significantly shorter than those of deflagration and the generic losses. Therefore, at the onset of detonation, there is local accumulation of energy that will take a significant amount of time to dissipate to return the domain to a natural state (longer than the time-of-flight of a traveling detonation wave). However, gain depletion is governed by simplified Arrhenius kinetics Eq. (2), where the base state of the domain, η, is now elevated because of the slow-scale energy dissipation. In effect, the weak restoring force acts to accelerate kinetics in the chamber. Analogous physical mechanisms in real engines include preheating of the propellant and insufficient expulsion of

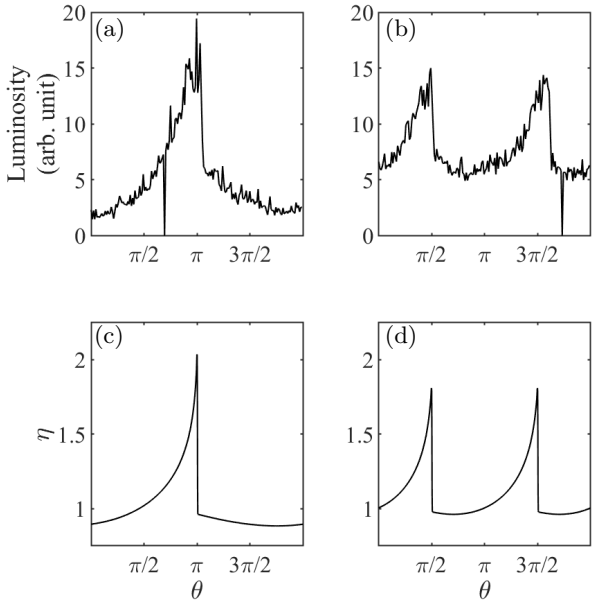

FIG. 10. Integrated pixel intensity displayed through θ for an experiment through which a mode transition from one (a) to two (b) waves occurs. A similar induced bifurcation in a simulation is displayed in (c) and (d). Of note is (i) the decrease of wave amplitude between one and two waves, (ii) the increase in background luminosity (or, in the simulation, base state of η), and (iii) the local increase of the magnitude of the state preceding the waves. The wave speeds decrease about 10% through the bifurcation, though this decrease is attributable to both a reduction in wave amplitude and an increase in parasitic deflagration. Once the parasitic deflagration can self-steepen to form a shock (see Fig. 8), a bifurcation of number of waves occurs.

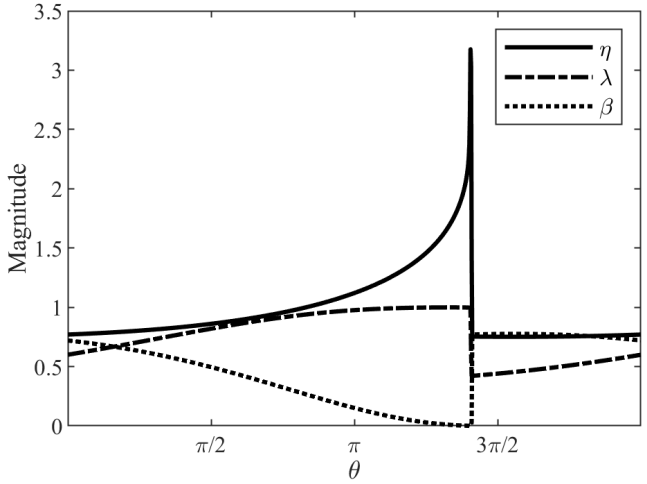

FIG. 11. Increasing the magnitude of the loss coefficient ϵ from 0.11 to 0.3 increases the traveling wave speed to 117% (up from 74%) of the CJ value referenced to an ambient state of $\eta_0 = 0$. The simulation is otherwise identical to that of Fig. 8.

burnt propellant from the combustion chamber. These phenomena lead to an increase of temperature in the domain and subsequently faster kinetics and an increased susceptibility to parasitic deflagration.

To exemplify this phenomena, Fig. 10 includes snapshots in time of the waveforms within the domains of an experiment and a simulation of the model system. Once parasitic deflagration preceding the detonation can self-steepen, a new wave is nucleated and begins the mode-locking process. With an additional wave, the base state of the domain is elevated further and parasitic deflagration is exacerbated. Although the wave speeds before and after bifurcations in the model system are comparable (on the order of 10% jumps in velocity), the developed speeds are the manifestation of both changes in wave amplitudes and the mean combustor state. Therefore, to increase wave speeds and proportion of heating via detonation (compared to deflagration) is analogous to increasing the strength of the restoring force. For example, increasing the restoring force coefficient from $\epsilon = 0.11$ to 0.3 of the simulation in Fig. 8 results in a single wave traveling at 117% of the CJ speed of the propellant (compared to two waves each traveling at 74% of the CJ speed). The waveform is shown in Fig. 11. Note that this is not an over-driven detonation but rather a reference to the CJ wave with a non-elevated base state of the domain ($\eta_0 = 0$).

C. Mode-locking and Bifurcations in Laser Systems

The electromagnetic field in an optical fiber laser cavity is described by the nonlinear Schrödinger equation (NLS) - a slowly-varying envelope field approximation that relates the dominant balance physics of wave dispersion and nonlinearity [8]. The NLS equation admits soliton solutions, or waveforms where nonlinearity and dispersive phenomena exactly balance, allowing for stable and steady wave propagation. In ring fiber lasers (Fig. 12), these soliton pulses are subject to localized *gain* and *loss*, as imposed on the system by an external energy feed source (pump) and energy sink (an output coupler and saturable absorber, for example).

In such laser configurations, the time scales of gain absorption can be significantly different than that of the gain recovery. The implication is that an *intensity discrimination* exists: the pulses in the cavity experience pulse-shaping phase shifts biased towards higher-intensity gain due to a saturable absorption mechanism [8]. In this manner, should multiple pulses exist in the system, the pulses establish a communication link via the gain and loss mechanisms. The pulses become mode-locked in that they experience phase shifts (once per round trip through the ring fiber) that adjust the inter-pulse spacing such that through time, the pulses experience equivalent amounts of gain [35].

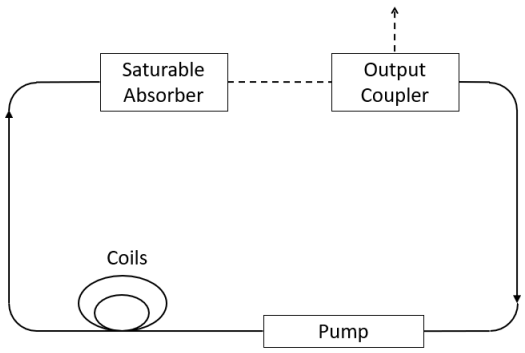

FIG. 12. Ring fiber laser configuration with localized gain (pump) and loss (output coupler where a fraction of the energy is directed out of the system). The collection of soliton pulses within the cavity are formed by the intensity discrimination (nonlinear loss) provided by the saturable absorber. The solitons seek maximal and symmetric phase differences between one another in an analogous process to that of rotating detonation waves.

Should the gain in the system be increased, the local balance of nonlinearity and dispersion no longer holds and the soliton is destabilized. Specifically, as a soliton pulse is subject to increasing gain, its spectral width grows beyond the gain bandwidth and becomes unstable. After a point of criticality, the pulse will destabilize and split into two separate pulses of lower amplitude and smaller bandwidth. These pulses become mode-locked through the same phase-shifting processes.

The balance between gain, losses, dispersion, and nonlinearity in the fiber ring laser system dictate the quasi-steady behavior of the pulses and the inter-pulse dynamics, including bifurcations. Each component of this canonical balance physics has an analogous counterpart in the RDE. The balance between dispersion and nonlinearity of the soliton pulse is analogous to the solitary detonation wave - a stably traveling wave whose shape is governed by heat release and injection dynamics. Laser cavity losses via dissipation and output coupling are analogous to ejection of energy through advection and/or heat conduction. The competition for gain between pulses is also present in both the laser cavity [35] and the RDE.

VI. CONCLUSION

The significance of the proposed model is twofold. First, although we claim no engineering predictive capabilities, our model does relate the dominant physics of gain depletion, gain recovery, and energy dissipation of rotating detonation waves in a simple mathematical framework that recovers, qualitatively, the nonlinear dynamics and bifurcation structure of these waves. Our model is a significant departure from the state-of-the-art computational fluid dynamic simulations of rotating detonation engines. However, this departure allows for a broad and comprehensive exploration of the physics governing wave behavior in a context that is hardware independent. Such an investigation is not currently feasible with high-fidelity, hardware-specific computational fluid dynamic simulations.

Second, the experimental observations and model extend the well-established physical phenomenon of mode-locking to rotating detonation waves. The energy balance in the RDE combustion chamber is generic, producing mode-locked states that interact through the global gain dynamics. These dominant balance physics are also observed in well-established laser systems where an analysis of the energy balance produces the global bifurcation structures [9]. Possessing knowledge of the mode-locking process and bifurcation structure of the waves is crucial to the development and deployment of the rotating detonation engine. Because the amount of performance-inhibiting parasitic deflagration is directly tied to the mode of operation, effective performance metrics can be defined (ratio of heating from detonation versus deflagration, for example) and optimized with respect to model parameters. Furthermore, although the presented model is primitive, stability criteria can be derived and actuation and control schemes can be conceptualized to drive the system to a stable, high-performing state.

ACKNOWLEDGMENTS

The authors acknowledge sponsorship under the Air Force Office of Scientific Research (AFOSR) grant FA 9550-18-1-9-007 and Office of Naval Research funding document N0001417MP00398. JNK acknowledges support from AFOSR grant FA9550-17-1-0329.

Appendix A: Control Volume Derivation

We follow a derivation process laid out by Mi and Higgins [32] with the key difference being our inclusion of a second dimension, as depicted in the control volume in Fig. 13. The aim is to capture the dynamics of an intensive property, here taken to be internal energy (denoted η), through time. The time rate of change of η in the control volume is equal to the difference in fluxes into and out of the volume. Additionally, a source term mimicking chemical heat release releases energy within the domain. Mathematically:

$$\begin{aligned}\dot{E}_{cv} = \Delta x \Delta y \left[q\dot{\lambda}\right] \\ +\Delta y \left[f\left(\eta_x\right) - f\left(\eta_{x+\Delta x}\right)\right] \\ +\Delta x \left[f\left(\eta_y\right) - f\left(\eta_{y+\Delta y}\right)\right],\end{aligned} \tag{A1}$$

where x and y are coordinates in the circumferential (periodic) and axial directions, respectively, q is the propellant specific heat release, λ is a combustion progress variable, and $f(\eta)$ is the flux of η across a boundary. The

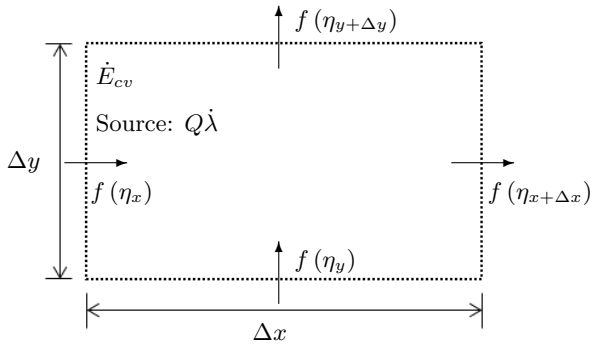

FIG. 13. 2-D control volume for model derivation.

property η is defined to be the specific internal energy $\frac{E}{\Delta x \Delta y}$.

Dividing by the dimensions of the control volume, one arrives at:

$$\dot{\eta}_{cv} = q\dot{\lambda} + \frac{f(\eta_x) - f(\eta_{x+\Delta x})}{\Delta x} + \frac{f(\eta_y) - f(\eta_{y+\Delta y})}{\Delta y}. \tag{A2}$$

As in Majda's original paper [6] and in Mi and Higgins' derivation [32], we choose the simplest flux to satisfy the convexity required for the Lax entropy condition; i.e., that $f(\eta) = \frac{1}{2}\eta^2$. Taking the limits as $\Delta x \to 0$ and $\Delta y \to 0$ and moving the spatial terms to the left hand side yields:

$$\frac{\partial \eta}{\partial t} + \frac{\partial \frac{1}{2}\eta^2}{\partial x} + \frac{\partial \frac{1}{2}\eta^2}{\partial y} = q\frac{\partial \lambda}{\partial t}. \tag{A3}$$

Appendix B: Quadratic Losses

Because of the restriction of the domain to the periodic 1-D line in the x co-ordinate, the axial (y) gradient will be modeled. The control volume is chosen to exist adjacent or attached to the front endwall of a RDE. At this front endwall, the flux of η entering the domain is assumed to have a negligible effect on the evolution of energy in the domain when compared to the circumferential flux terms and source term. As such, $f(\eta_y) = f(\eta_{y=0}) \approx 0$, so the approximation of the gradient becomes:

$$\frac{\partial \frac{1}{2}\eta^2}{\partial y} \approx \lim_{\Delta y \to 0} \frac{\frac{1}{2}\eta^2_{y+\Delta y} - 0}{\Delta y}. \tag{B1}$$

To simplify further, we assume that the detonation waves in real engines are approximately planar and the properties immediately before and after the passage of a wave are approximately uniform. Therefore, we assume that from the axial location $y = 0$ (attached to the front end wall of the engine) to $y = y_c$ (where y_c is the height of the detonation wave) the properties are uniform. Exploiting this approximate uniformity, the limit of Eq. (B1) is taken to $\Delta y \to y_c$ (instead of zero). Any further reduction in the value of Δy will, in effect, over-predict the magnitude of the gradient. This simplified limit now takes on a polynomial form:

$$\lim_{\Delta y \to 0} \frac{\frac{1}{2}\eta^2_{y+\Delta y}}{\Delta y} \approx \lim_{\Delta y \to y_c} \frac{\frac{1}{2}\eta^2}{\Delta y} = \epsilon_0 \frac{1}{2}\eta^2 = \epsilon\eta^2, \tag{B2}$$

where $\epsilon = \frac{1}{2}\epsilon_0$ are constants reflecting the severity of the axial gradient of flux through the engine. Note that the flux function $f(\eta) = \frac{1}{2}\eta^2$ acts as an equation of state relating the property η to another whose gradient drives flow - this derived property $\frac{1}{2}\eta^2$ is analogous to pressure in the momentum equation for fluid flows. In real engines whose axial flow is thermally choked (the Mach number at the exit of the engine is 1), the axial pressure gradient near the front wall of the RDE is proportional to pressure at that location; i.e. $\frac{\partial p}{\partial y}|_{y=0} = cp_{y=0}$, where c is some parameter intrinsic to the engine. Experimental evidence supports this assumption - for this we refer to [36]. The proposed functional form of the axial gradient in Eq. (B2) enforces the same behavior.

The equation governing the evolution of energy in the circumferential domain is now given as:

$$\frac{\partial \eta}{\partial t} + \eta\frac{\partial \eta}{\partial x} = q\frac{\partial \lambda}{\partial t} - \epsilon\eta^2. \tag{B3}$$

This is equivalent to the inviscid Burgers' Equation with a chemical reaction source term and loss of energy to an ambient condition. The physical mechanism for the loss is the lateral relief from lack of confinement on one side of the traveling waves. Regularization with a viscous term ($\nu\frac{\partial^2 \eta}{\partial x^2}$) completes the comparison to the classic Burgers' equation, though for this study we exclude viscous effects.

[1] B. A. Rankin, M. L. Fotia, A. G. Naples, C. A. Stevens, J. L. Hoke, T. A. Kaemming, S. W. Theuerkauf, and F. R. Schauer, J. Prop. Power **33**, 131 (2017).
[2] C. A. Nordeen, D. Schwer, F. Schauer, J. Hoke, T. Barber, and B. Cetegen, Combustion, Explosion, and Shock Waves **50**, 568 (2014).
[3] V. Anand, A. S. George, R. Driscoll, and E. Gutmark, Int. J. Hydro. Energy **40**, 16649 (2015).

[4] V. Anand, A. S. George, and E. Gutmark, Int. J. Hydro. Energy **42**, 12629 (2017).
[5] J. W. Bennewitz, B. R. Bigler, J. J. Pilgram, and W. A. Hargus, Int. J. Ener. Mat. Chem. Prop. **18**, 91 (2019).
[6] A. Majda, SIAM J. Appl. Math. **41**, 70 (1981).
[7] H. A. Haus, IEEE J. Sel. Top. Quan. Elec. **6**, 1173 (2000).
[8] J. N. Kutz, SIAM Review **48**, 629 (2006).
[9] F. Li, P. Wai, and J. N. Kutz, JOSA B **27**, 2068 (2010).
[10] R. E. Cullen, J. A. Nicholls, and K. W. Ragland, J. Spacecraft and Rockets **3**, 893 (1966).
[11] F. A. Bykovskii, S. A. Zhdan, and E. F. Vedernikov, J. Prop. Power **22**, 1204 (2006).
[12] M. Bohon, R. Bluemner, C. Paschereit, and E. Gutmark, Experimental Thermal and Fluid Science **102**, 28 (2019).
[13] S. Liu, W. Liu, Z. Lin, and W. Lin, Combustion Science and Technology **187**, 1790 (2015).
[14] V. Anand and E. Gutmark, Progress in Energy and Combustion Science **73**, 182 (2019).
[15] S. Prakash, R. Fiévet, V. Raman, J. Burr, and K. H. Yu, AIAA Journal , 1 (2019).
[16] M. Hishida, T. Fujiwara, and P. Wolanski, Shock Waves **19**, 1 (2009).
[17] Y.-T. Shao, M. Liu, and J.-P. Wang, Combustion Science and Technology **182**, 1586 (2010).
[18] D. Schwer and K. Kailasanath, Proc. Comb. Inst. **33**, 2195 (2011).
[19] R. Zhou and J.-P. Wang, Shock Waves **23**, 461 (2013).
[20] K. M. Spaulding, D. H. Yong, A. D. Kim, and J. N. Kutz, JOSA B **19**, 1045 (2002).
[21] J. N. Kutz, Physica D: Nonlinear Phenomena **238**, 1468 (2009).
[22] N. A. Adrian Ankiewicz, ed., *Dissipative Solitons: From Optics to Biology and Medicine* (Springer Berlin Heidelberg, 2008).
[23] M. C. Cross and P. C. Hohenberg, Reviews of Modern Physics **65**, 851 (1993).
[24] J. A. Boening, E. A. Wheeler, J. D. Heath, J. V. Koch, A. T. Mattick, R. E. Breidenthal, C. Knowlen, and M. Kurosaka, J. Prop. Power **34**, 1364 (2018).
[25] J. W. Bennewitz, B. R. Bigler, S. A. Schumaker, and W. A. Hargus, Review of Scientific Instruments **90**, 065106 (2019).
[26] W. Fickett, in *The Mathematics of Combustion* (SIAM, 1985) pp. 133–181.
[27] R. R. Rosales and A. Majda, SIAM J. Appl. Math. **43**, 1086 (1983).
[28] L. M. Faria, A. R. Kasimov, and R. R. Rosales, J. Fluid Mech. **784**, 163 (2015).
[29] G. Lyng and K. Zumbrun, Physica D: Nonlinear Phenomena **194**, 1 (2004).
[30] V. A. Vasilev, Y. M. Romanovskiii, and V. G. Yakhno, Soviet Physics Uspekhi **22**, 615 (1979).
[31] B. S. Kerner and V. V. Osipov, Soviet Physics Uspekhi **32**, 101 (1989).
[32] X. Mi and A. J. Higgins, Physical Review E **91** (2015), 10.1103/physreve.91.053014.
[33] D. I. Ketcheson, K. Mandli, A. J. Ahmadia, A. Alghamdi, M. Q. de Luna, M. Parsani, M. G. Knepley, and M. Emmett, SIAM Journal on Scientific Computing **34**, C210 (2012).
[34] B. G. Bale, K. Kieu, J. N. Kutz, and F. Wise, Optics Express **17**, 23137 (2009).
[35] J. N. Kutz, B. Collings, K. Bergman, and W. Knox, IEEE Journal of Quantum Electronics **34**, 1749 (1998).
[36] J. Koch, M. R. Washington, M. Kurosaka, and C. Knowlen, in *AIAA Scitech 2019 Forum* (American Institute of Aeronautics and Astronautics, 2019).